Theoretical study of the structure and electronic spectra of fully protonated emeraldine oligomers

ARTICLE *in* INTERNATIONAL JOURNAL OF QUANTUM CHEMISTRY · JULY 2007

Impact Factor: 1.43 · DOI: 10.1002/qua.21241

5 AUTHORS, INCLUDING:

Hristina R Zhekova
The University of Calgary
12 PUBLICATIONS **143** CITATIONS
SEE PROFILE

A. Tadjer
Sofia University "St. Kliment Ohridski"
65 PUBLICATIONS **425** CITATIONS
SEE PROFILE

Theoretical Study of the Structure and Electronic Spectra of Fully Protonated Emeraldine Oligomers

H. ZHEKOVA,[1] A. TADJER,[1] A. IVANOVA,[1] J. PETROVA,[1] N. GOSPODINOVA[2,3]

[1]*Faculty of Chemistry, University of Sofia, 1 J. Bourchier Ave, 1126 Sofia, Bulgaria*

[2]*Laboratoire de Chimie Macromoléculaire, Ecole Nationale Supérieure de Chimie de Mulhouse, 3 rue Alfred Werner, 68093 Mulhouse Cedex, France*

[3]*Institut de Chimie des Surfaces et Interfaces, 15, rue Jean Starcky, BP 2488, 68057 Mulhouse Cedex, France*

Received 24 July 2006; accepted 13 September 2006
Published online 31 October 2006 in Wiley InterScience (www.interscience.wiley.com).
DOI 10.1002/qua.21241

ABSTRACT: Polyaniline (PANI) is one of the most studied conducting polymers. Obtained in its conducting form (known as "emeraldine salt") by chemical or electrochemical oxidation of aniline in aqueous acidic medium, this polymer manifests an array of attractive properties. Nevertheless, these properties still need to be described at the molecular level. Intense theoretical investigations during the past few years aim at explaining the chain organization, conductivity mechanism, and other structural and spectral characteristics. Most studies adopt simplified models in which hydration effect is underestimated, since all simulations are performed either in vacuum or in the presence of a limited number of water molecules. The present computational study sheds light on the molecular organization of a number of model PANI hydrated clusters with different alignment and multiplicity, which can explain the experimentally recorded UV/VIS spectra. The influence of hydration and interaction with adjacent oligomers is estimated. Short-chain doubly protonated emeraldine oligomers are used as model systems. The calculations are performed at the semi-empirical (AM1) and/or molecular mechanics (AMBER96) level. Proper configurations of the clusters are selected using Monte Carlo simulations. Electron correlation (CIS) is accounted for upon evaluation of the absorption spectra of the clusters. The relative strength of the interchain coupling is estimated by simulation of PANI clusters consisting of two PANI tetramers in water. Comparison to experimental results is made.

Key words: polyaniline; emeraldine salt; UV/VIS/NIR electron spectra; semi-empirical calculations; molecular mechanics simulations; stacking; hydration

Correspondence to: A. Tadjer; e-mail: tadjer@chem.uni-sofia.bg
Contract grant sponsor: National Science Fund at the Bulgarian Ministry of Education and Science.
Contract grant number: BY318/06.

1. Introduction

Polyaniline (PANI) is among the most extensively studied systems during the past two decades. It exists in several forms (Fig. 1) that differ in oxidation state [1]. The fully reduced PANI is called leucoemeraldine base (LEB) and is nonconductive; it is a chain of aniline residues with amino nitrogen atoms. Absence of conductivity also is observed in the fully oxidized form, pernigraniline (PNB), with imino nitrogens. The third form, emeraldine base (EB), is semi-oxidized and features alternation of two amino and two imino nitrogen atoms per unit cell (tetramer). These forms can be obtained by appropriate postpolymerization treatment of emeraldine salt of PANI: reduction, oxidation, and deprotonation. The application-oriented conductive emeraldine salt (ES) features conductivity of the order of $\sim 10^2$ S/cm [2, 3].

Various applications of PANI as an emeraldine salt form or in its undoped forms are known [4]. PANI displays attractive thermochromic and solvatochromic properties [5–7]. PANI complexes with different transition metals are used for the production of electrochromic glasses [8]. The diversity of electronic properties of polyanilines makes them potential and actual components in numerous devices [9]. The application of PANI in different types of batteries [10] or in conducting antistatic films [11] has already been brought to the industrial stage. This is only part of the myriad of PANI applications, those that have immediate relevance to this study.

Electron density distribution of PANI is determined by bond length and by the magnitude of dihedral angles. The latter stems from the steric interactions of the adjacent benzene rings in the polymer [12–15] and controls the π-delocalization along the chains and, consequently, the intrachain mobility of charge carriers, affecting PANI electronic properties. The utilization of this torsion flexibility is critical for the construction of various optical memory devices [16].

The unusual combination of color, conductivity, and synthetic availability, along with the prospect for practical applications, is the major reason for the lasting interest in the physics and chemistry of PANI systems. The theoretical investigations dedicated to PANI are also plentiful and cover almost all computational levels, i.e., molecular mechanics and dynamics [17] (doping mechanism, proton migration, temperature dependence of absorption, and conductivity), Monte Carlo [18, 19] (interchain electronic transport in disordered systems), Hückel [20] (band structure, DOS), semi-empirical methods [21, 22] (structure, UV/VIS spectra), as well as first-principle methods such as Hartree–Fock and DFT [23–28] (structure, infrared and Raman spectra). Some semi-empirical calculations are performed for the evaluation of torsion barriers and solvation effects on the UV/VIS spectra of PANI chains, accounted for by models including 2 to 4 solvent molecules [29, 30]. The main part of these computations was performed for species with artificially augmented symmetry by means of end-capping of the chains with identical residues. This facilitates the calculations but leads to inaccurate description of the properties for which the end effects are crucial. The absence or deficiency of water molecules significantly decreases the plausibility of the models and makes dubious the adequate comparison between theory and experiment. Thus, the search of better models, which take into account the end and solvation effects, is of great importance for the rationalization of theoretical results. In our previous studies [31], some of the mentioned drawbacks are corrected by design of model clusters of hydrated asymmetric non- and mono-protonated tetramers, where the water is accounted for explicitly (~100 molecules per oligomer). In this article, we keep to the same calculation scheme and extend the range of our studies on doubly protonated emeraldine tetramers (DPE), which are models of the form responsible for PANI conductivity, i.e., the emeraldine salt.

Stacks of doubly protonated emeraldine (DPE) tetramers of different multiplicity are considered. The results are discussed in terms of energetics,

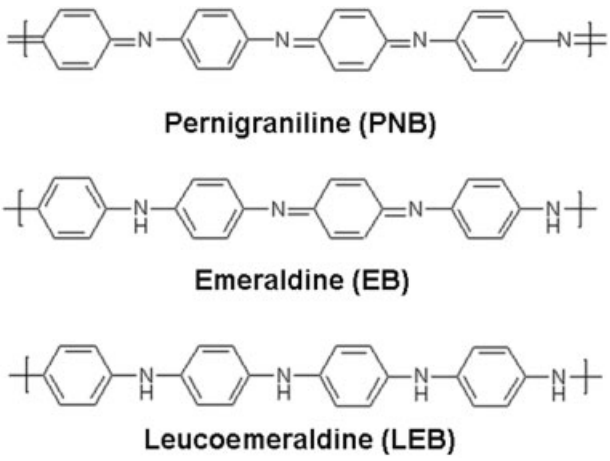

FIGURE 1. Chemical formulae of PANI forms.

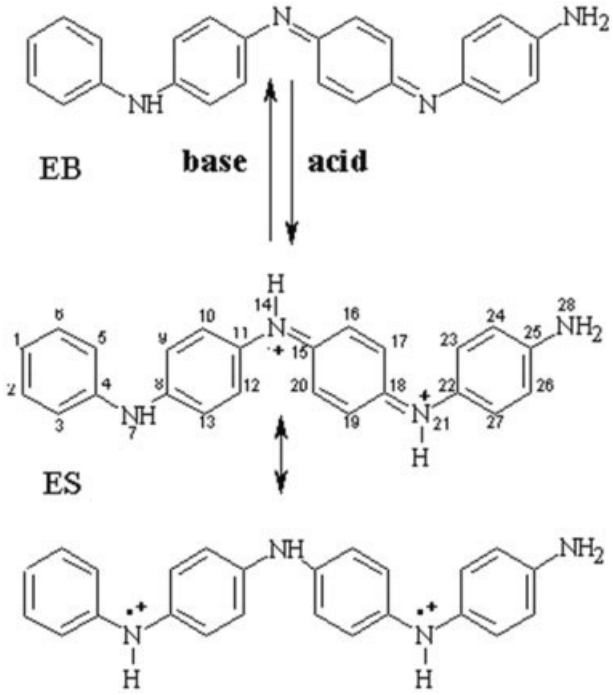

FIGURE 2. Doubly protonated emeraldine tetramer (DPE). The protonated nitrogens are numbers 14 and 21.

structural parameters, and spectral behavior, the latter being indicative of conduction potential. The computed estimates are compared with experimental spectra. The simulations allow description of the driving forces of oligomer ordering. Speculations on the relationship between ordering/compactness and optical transition probability/conductivity are made.

2. Computational Details

2.1. MOLECULAR MODELS

Correct topology is the foremost requirement for reliable molecular modeling. It is known that the imino:amino nitrogen ratio in the emeraldine base is 1:1. As this does not define the sequence of N-atom oxidation states in the chain, Figure 2 represents the topology adopted in this study based on the structures cited most often in the relevant bibliography [1].

Protonation of the imino nitrogen atoms in emeraldine base can occur upon exposure to strong acids [31]. Since amino groups have basic properties that are even weaker than those of ammonia, only imino nitrogen atoms are assumed protonated in the models. Owing to the nonidentical atomic charges (Table I) of the two imino groups, protonation in the tetramer can be carried out in two stages leading to partially or fully protonated emeraldines. The theoretical study of partially protonated emeraldine systems has already been described in a previous work [31]. In the present article we extend the range of our investigations by taking into consideration the structural and spectral properties of fully (doubly) protonated emeraldine tetramers and the interchain interaction modeled as two stacked molecules.

Another essential factor accounted for in the models is the possibility for the existence of spin-active DPE states. The abundant EPR results [23, 32–38] prove that the emeraldine salt of PANI is a system in which states of different multiplicities can be detected. In some of their works Epstein and co-workers [39–41] develop a theory based on the

TABLE I
AM1 Mulliken atomic charges of singlet and triplet DPE tetramers.*

Skeletal atom no./ multiplicity	1	2	3	4	5	6	7	8	9	10
Singlet	0.077	0.006	0.065	−0.015	0.035	0.032	0.155	0.225	−0.070	0.316
Triplet	0.055	−0.006	0.039	0.032	0.020	0.029	0.108	0.125	−0.018	0.201
Skeletal atom no./ multiplicity	11	12	13	14	15	16	17	18	19	20
Singlet	0.052	0.136	−0.055	0.450	−0.221	0.075	0.061	0.142	−0.086	0.084
Triplet	0.184	0.008	−0.008	0.195	−0.001	0.014	0.059	0.019	0.022	−0.009
Skeletal atom no./ multiplicity	21	22	23	24	25	26	27	28		
Singlet	0.285	−0.049	0.060	−0.112	0.148	−0.091	0.215	0.080		
Triplet	0.190	0.208	0.094	−0.056	0.154	−0.032	0.158	0.217		

* The charges of the hydrogen atoms are condensed to the heavy atoms they are bonded to.

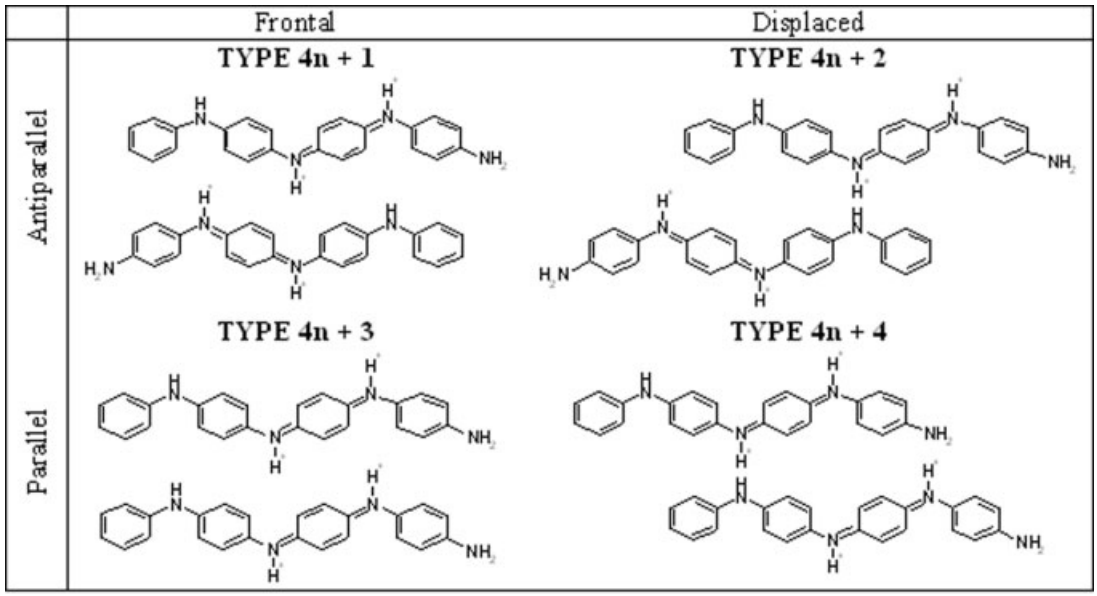

FIGURE 3. Schematic representation and designation convention of the DPE stacks studied; $n = 0, 1, 2$.

assumption of spin density localization in the vicinity of the protonated nitrogen atoms. This leads to the conclusion that for the doubly protonated emeraldine tetramers there are two possible ground states: singlet and triplet. The geometry of these structures, obtained after AM1 optimization in vacuum, is similar but their charge distribution varies substantially (Table I).

The values listed in Table I demonstrate the difference between the singlet and triplet atomic charges, which will have an impact on their structural and spectral properties. The AM1 geometry in vacuum is not discussed in this article, since it undergoes noticeable changes in the presence of chloride anions, which are employed as counterions in the current computations. The geometry of the DPE clusters will be described in the corresponding sections. The choice of realistic initial charges is of great importance for the aqueous solution simulations carried out with molecular force fields. Therefore, calculations with both charge distributions in Table I are performed.

The experimental polymerization conditions encompass an active medium formed by water molecules, monomer, acidifying and oxidizing agents, and nearby oligomer chains. The environmental effect should be taken into account when simulating the UV spectrum of the emeraldine salt. For the sake of effective comparison with the experimental data available, calculations for single tetramers and stacks of tetramers are carried out both in vacuum and in water.

The stacks are constructed from two doubly protonated emeraldine tetramers with various mutual orientation and ground-state multiplicity. With respect to spatial organization, 12 possible types of stacks are formed by tetramers with parallel or antiparallel configuration, with or without chain displacement, with identical or different multiplicity. Estimation of the ground-state multiplicity in vacuum of single tetramers and all stacks studied (Fig. 3) is made at the AM1 level with CAS(10,10) [42]. The calculations are done in the absence of chloride counterions in order to include only PANI orbitals in the active space. The results are presented in Table II.

Obviously, the energy differences between the possible spin-states of a particular structure are $\sim 10^{-2}$ eV (0.24 kcal/mol). This insignificant energy splitting is an indication for the coexistence of structures of different multiplicity. This fact is taken into consideration in the computational scheme for the UV spectra simulation.

MOPAC96/AM1/CAS(10,10) calculations for the structures most similar to the ones investigated in this study (the monoprotonated emeraldine single chain and stacks) provide singlet–triplet splitting of the order of 0.8–1.0 eV in favor of the singlet. Therefore, in this half-protonated system, the prob-

TABLE II

AM1/CAS(10, 10) correlation corrections to the SCF total energies for the different spin states of the studied systems.

Structure	Relative energy (eV)		
	Singlet	Triplet	Quintet
Singlet	−2.83851	−2.85601	—
Triplet	−2.87448	−2.85519	—
Stack type 1	—	−5.28647	−5.37198
Stack type 2	−5.68609	−5.74562	−5.26712
Stack type 3	—	−5.44453	−5.51414
Stack type 4	−5.81011	−5.81012	−5.84862
Stack type 5	—	−5.53328	−5.57335
Stack type 6	−5.49783	−5.54253	−5.36003
Stack type 7	−5.27335	−5.24042	−5.28851
Stack type 8	−5.62161	−5.63023	−5.61829

ability of the existence of higher-multiplicity structures is insignificant.

Accounting for the dual ground-state multiplicity of the single DPE tetramer, three possible spin-states are presumed for the stacks, i.e., singlet, triplet, and quintet. More detailed description will be made in the corresponding sections.

2.2. COMPUTATIONAL SCHEME

The initial structures of the doubly protonated tetramers used for stacks/hydration shell construction are acquired from AM1 geometry optimization (gradient 0.01 kcal/mol. Å) in vacuum. Both the singlet and triplet species are optimized separately, thus forming the two basic model chains, i.e., a singlet and a triplet one, which differ in charge distribution (Table I). The chloride counterions are added to the optimized tetramers at 3.5 Å from the corresponding protons followed by a new force field geometry optimization (gradient 0.01 kcal/mol. Å) with C—C bonding parameters in AMBER96 modified to reproduce correctly the structure of the quinoid rings [31, 43]. The AMBER96 optimized structures are then used for the construction of all clusters. They are preferred to the AM1 optimized ones because their geometry is more realistic due to the possibility of optimizing the tetramer in the presence of counterions.

For the stack assembly, the two tetramer chains are put at 3 Å from each other, as prescribed in the literature sources [31]. The mutual orientation of the chains is dictated by maximum overlap requirement between benzene and quinoid rings. Attraction forces are expected between the electron density-abundant quinoid and electron density-deficient benzene rings [44], which should stabilize the stacked structures. Before their hydration, the stacks are subject to AMBER96 geometry optimization (gradient 0.01 kcal/mol. Å) in vacuum.

Hydration effects are investigated in a number of solvated clusters consisting of one DPE tetramer or a stack of two oligomers immersed in 197 or 394 water molecules, respectively, together with the counterions. To simulate periodic boundary conditions, periodic boxes with sizes $18 \times 18 \times 30$ Å (for the single tetramer chains) and $20 \times 20 \times 35$ Å (for the stacks) are used. The solvent is accounted for explicitly with the TIP3P model. Metropolis Monte Carlo simulation at 300 K, with outer cutoff radii of 9 and 10 Å (for both box sizes) is carried out to minimize system energy. After relaxation (~40,000 MC steps for the single hydrated tetramers and 100,000 for the stacks), 15–18 low-energy structures are chosen from the relaxed part of the MC trajectory, and their geometries (including the solvent molecules and the counterions) are optimized with AMBER96 (gradient 0.1 kcal/mol. Å). The structures are then used for UV spectra simulation and geometric parameters evaluation.

Simulation of the UV spectra is performed with AM1/CIS. This method calculates slightly enhanced electron correlation due to its parametrization adjusted to fit experimental values at SCF level, but it still provides correct description of some qualitative tendencies in the optical properties of the systems within acceptable computational time. Besides, AM1/CIS has proved its applicability for the adequate experimental UV spectra simulation of some conjugated π-systems of similar nature [45].

The optical transitions are obtained with AM1/CIS(10,10) (10 polyaniline orbitals) for the single emeraldine tetramers and AM1/CIS(20,20) for the stacks. The multiplicity is specified in the SCF procedure, which precedes the calculation of the CI matrix. The obtained values for the structural and spectral parameters are averaged over the entire low-energy series.

The calculations are carried out with the HyperChem 7 program package [46]. The CAS simulations are performed with an extended version of MOPAC93 [47].

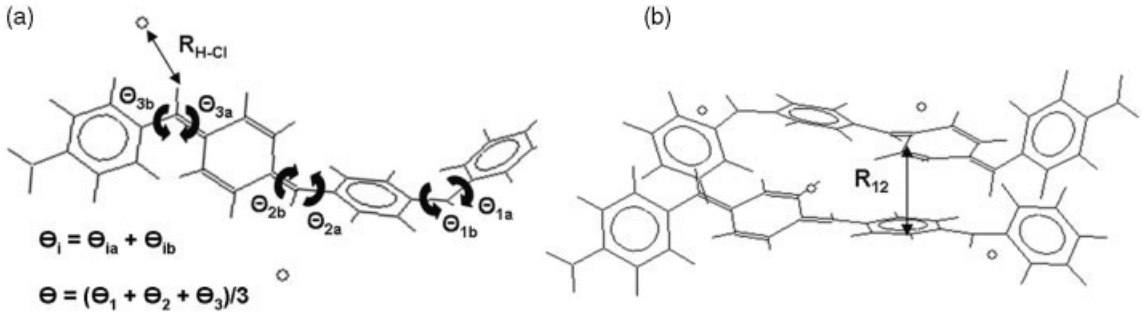

FIGURE 4. AMBER96 optimized geometry. (a) a single DPE tetramer; (b) stack of two tetramers. Notations of the dihedral angles between adjacent benzene rings Θ_i, the distance between the chloride ions and their corresponding protons $R_{H\text{—}Cl}$, and the intermolecular distance in the stacks R_{12} are provided.

3. Results and Discussion

3.1. STRUCTURES OF TETRAMERS WITH SINGLET INITIAL CHARGE DISTRIBUTION

The results for single tetramers and stacks built thereof in vacuum and water are described in this section. Figure 4(a) presents a single singlet emeraldine tetramer with its chloride counterions after AMBER96 geometry optimization.

There are four possible stacked structures complying with the requirements listed in Section 2.2. The AMBER96 optimized geometries of singlet-DPE stacks are illustrated in Figure 5. These four stacking patterns are expected to provide the strongest interaction of the oligomers. The remaining chain alignments will not be addressed in the present work, as they correspond to PANI obtained in experimental conditions different from our reference substances. Table III presents

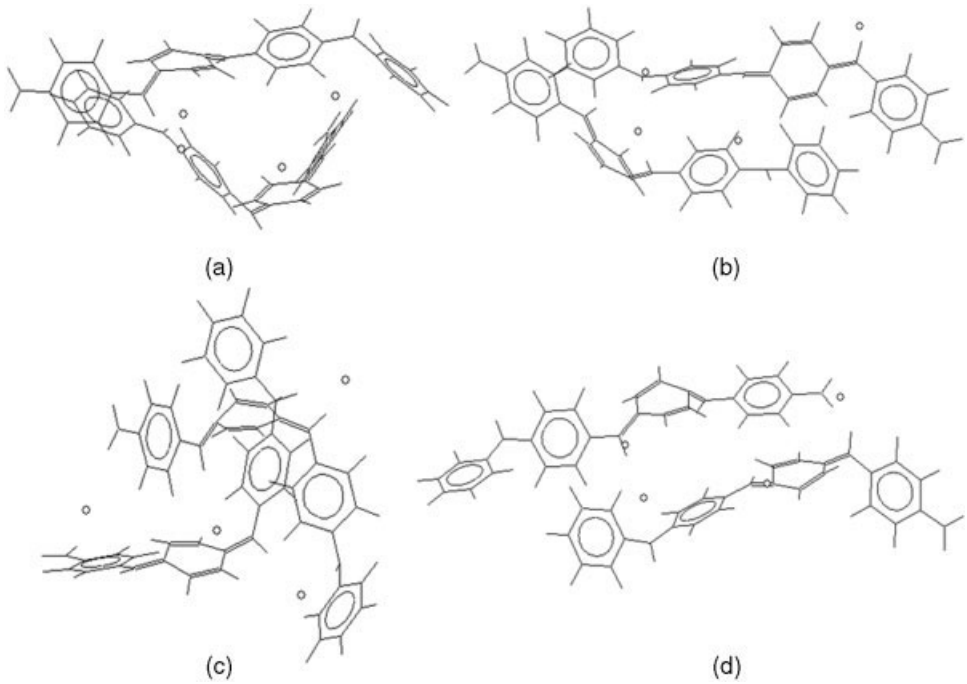

FIGURE 5. AMBER96 optimized geometry of stack type 1 (a), type 2 (b), type 3 (c), and type 4 (d) in vacuum, side view.

TABLE III

Average structural parameters of all DPE systems studied.*

Structure	Θ (°)		$R_{H\text{-}Cl}$ (Å)		R_{12} (Å)	
	Vacuum	Water	Vacuum	Water	Vacuum	Water
Singlet	64.81	64.71	2.20	3.02	—	—
Triplet	54.13	57.64	2.00	2.87	—	—
Stack type 1	62.18	59.46	2.24	3.18	3.60	3.35
Stack type 2	56.95	54.01	2.24	2.99	3.64	3.29
Stack type 3	63.66	59.97	2.27	3.19	3.76	3.46
Stack type 4	66.34	73.31	2.21	2.91	3.66	3.64
Stack type 5	60.82	56.31	2.21	2.52	3.31	3.28
Stack type 6	62.66	61.66	2.25	3.51	3.58	3.45
Stack type 7	63.19	63.37	2.26	4.03	3.64	3.43
Stack type 8	62.34	66.60	2.26	2.56	3.70	3.72
Stack type 9	65.74	73.43	2.25	3.13	4.10	3.97
Stack type 10	62.48	68.02	2.22	2.66	3.53	3.38
Stack type 11	65.99	56.12	2.97	3.61	3.55	3.23
Stack type 12	64.82	64.01	2.24	2.67	3.33	3.29

* Θ, torsion angle; $R_{H\text{-}Cl}$, distance between a proton and its corresponding chloride counterion; R_{12}, distance between the tetramer chains in the stack regions of sizeable interchain overlap (see Fig. 4).

some structural descriptors for all models in this work.

Θ_i is the dihedral angle between each pair of adjacent phenyl rings and is an important parameter of the molecular geometry deformation, the latter being a crucial factor for the UV spectrum of the systems. The values of Θ in Table III are averaged over the three Θ_i.

$R_{H\text{—}Cl}$ is the distance between the proton of the protonated imino nitrogen and its corresponding chloride counterion. R_{12} is the distance between the tetramer chains in the stack and is calculated by averaging of distances between pairs of closest-contact atoms in the DPE skeleton in the areas of chain overlap. $R_{H\text{—}Cl}$ and R_{12} are indices of the aggregate compactness.

The significant number of charged sites in the doubly protonated emeraldine systems determines their considerable hydration. This is the reason for the chloride ion drift away from the polyaniline tetramers in the DPE stacks. The intermolecular distance R_{12} demonstrates the opposite tendency; that is, it decreases after hydration (the stacks become more compact). This is natural as the PANI skeleton, except for its nitrogen-containing groups, is hydrophobic.

The environment influences the DPE geometry in stack types 1–4 too; it can be seen that the dihedral angles between the planes of adjacent rings decrease under the influence of water and nearby polyaniline chains, i.e., hydration and stacking "flatten" the systems. The only exception is stack type 4 featuring enhanced chain twisting in aqueous medium. The probable reason is the repulsive packing energy in this case (see below). Thus, the increased distortion eases the repulsion between the two chains. On the other hand, Θ is an average characteristic; its large value in stack type 4 is actually due to the twisted loose terminal rings, an effect that vanishes for longer chains.

The energy change attributable to interaction with water and/or interaction with other tetramers can be used as a quantitative measure of the medium influence on the polyaniline systems. Table IV presents the AMBER96 calculated total energies of the studied structures, as well as the corresponding molecular mechanics contributions to the steric energy: from bonds (E_b), valence angles (E_a), torsion angles (E_d), van der Waals (E_{vdw}), and electrostatic (E_{es}). The calculated energy of hydration (E_{hydr}) and stacking (E_{stack}) of all investigated structures are presented in Table V. They will be examined in detail in the corresponding sections.

The results shown in Table IV permit comparison of the investigated systems in vacuum and in water. The energy calculations can be carried out with or without taking the chloride ions into account. Since the chloride ions have small impact on the steric interactions in the systems, their influence on the terms accounting for the van der Waals exchange is insig-

TABLE IV

AMBER96 total energy and its contributions for all systems studied in vacuum and in water.*

	E_b (kcal/mol)		E_a (kcal/mol)		E_d (kcal/mol)		E_{vdw} (kcal/mol)		E_{el} (kcal/mol)		E_{tot} (kcal/mol)	
Structure	Vacuum	Water	Vacuum	Water	Vacuum	Water	Vacuum	Water	Vacuum	Water	Vacuum	Water
Singlet	1.34	0.74	3.06	5.79	10.71	13.72	24.85	−13.37	−186.23	−243.58	−146.26	−236.70
Triplet	1.16	0.96	3.47	3.75	10.44	13.79	23.62	−13.24	−182.64	−222.42	−143.95	−217.15
Type 1	1.33	1.20	4.48	6.95	12.48	13.75	18.55	−19.52	−320.15	−301.54	−283.31	−299.16
Type 2	1.53	0.97	5.68	6.58	13.77	16.31	19.46	−19.57	−299.02	−313.63	−258.58	−309.32
Type 3	1.42	1.04	4.53	4.27	14.30	18.54	19.11	−10.80	−315.26	−313.22	−275.89	−300.16
Type 4	1.28	1.02	3.68	6.09	12.01	17.54	18.01	−12.13	−291.20	−298.43	−256.21	−286.16
Type 5	1.13	0.82	4.92	6.10	9.73	12.24	15.49	−16.58	−291.08	−262.35	−259.81	−259.77
Type 6	1.09	0.93	3.06	4.77	18.15	22.38	17.80	−7.44	−288.24	−273.31	−248.14	−252.67
Type 7	1.08	0.69	2.52	4.15	17.34	20.95	15.09	−12.18	−289.00	−269.74	−252.97	−256.13
Type 8	1.20	0.76	3.50	3.55	12.61	15.35	19.50	−20.93	−288.52	−267.52	−251.70	−268.79
Type 9	1.21	0.85	2.98	2.92	11.36	16.74	18.21	−18.38	−286.67	−287.00	−252.92	−284.87
Type 10	1.21	1.03	4.56	5.81	12.67	14.88	17.06	−19.77	−285.44	−285.79	−249.94	−283.85
Type 11	1.26	1.00	3.82	5.22	13.96	13.90	18.81	−16.28	−308.71	−294.92	−270.86	−291.09
Type 12	1.23	0.73	3.09	2.55	10.89	19.21	19.31	−21.09	−302.92	−288.08	−268.41	−286.69

* Values are scaled per one PANI tetramer.

nificant. In fact, their only sizeable contribution is to the total energy of the structures due to the strong electrostatic attraction to the charged polyaniline chains and polar water molecules. The latter is considerable and obscures the adequate estimation of PANI energy contributions that are essential for hydration and stacking effects analysis. For this reason, the energy terms in Tables IV and V are estimated without participation of the chloride ions.

TABLE V

Calculated energy of hydration (E_{hydr}) [Eq. (1)] and stacking (E_{stack}) [Eq. (2)].*

Structure	E_{hydr} (kcal/mol)	E_{stack} (kcal/mol)
Singlet	−90.44	—
Triplet	−73.21	—
Stack type 1	−15.69	−6.16
Stack type 2	−50.75	−6.20
Stack type 3	−24.27	2.57
Stack type 4	−29.96	1.25
Stack type 5	0.04	−3.34
Stack type 6	−4.53	5.80
Stack type 7	−3.16	1.06
Stack type 8	−17.09	−7.70
Stack type 9	−31.96	−5.08
Stack type 10	−33.90	−6.47
Stack type 11	−20.23	−2.98
Stack type 12	−18.28	−7.79

* Values are scaled per one PANI tetramer.

As can be expected, hydration stabilizes substantially the PANI structures. The hydration energies are calculated using the following relation:

$$E_{hydr} = E_{tot}[\text{structure(s) in water}] - E_{tot}[\text{structure(s) in vacuum}]. \quad (1)$$

The largest value of E_{hydr} among the singlet clusters is found for stack type 2 and corresponds to the best hydration due to the small torsion angle Θ; the stack geometry facilitates the water molecule access to its surface, and especially to the terminal amino groups.

The change in the bonding contributions is insignificant; the slight decrease in PANI skeleton deformation grade upon hydration becomes the reason for the bond strain compensation at the expense of more strenuous valence and torsion angles. The van der Waals component of the energy undergoes substantial change and becomes attractive. Actually, E_{vdw} gives the most distinct quantitative description of the stacking effects, whose interpretation through E_{tot} is hampered by the large electrostatic contributions due to the aqueous envelope formed around the charged particles in the system. For this reason, the stacking energy (E_{stack}) calculation is based on the hydrated systems van der Waals energy. The E_{stack} evaluation is made according to eq. (2):

$$E_{\text{stack}} = E_{\text{vdw}}\,(1\ \text{DPE in hydrated stack}) - E_{\text{vdw}}\,(1\ \text{hydrated DPE tetramer}). \quad (2)$$

Thus, stack types 1 and 2 are 12.31 and 12.40 kcal/mol more stable than the single tetramer, respectively; i.e., the stacking is energetically favorable for these systems. Besides, stack type 2 is the most stable and most compact of all structures investigated (its energy is ~20 kcal/mol lower than the energy of stack type 1). Its overall stabilization results from the simultaneous enhancement of both van der Waals and electrostatic interactions in the aqueous medium. Moreover, the shape of the stack corresponds to the most stable stacked assembly of singly protonated emeraldine tetramers [31].

The situation for the other two stacks is the opposite; that is, the stacking increases their energy with 5.14 and 2.49 kcal/mol for stack types 3 and type 4, respectively. In accordance with this, the two tetramers in the former stack feature very distorted geometry, while in the latter the unfavorable atomic contacts are reduced by increase of the phenyl-phenyl torsion angles (Table III). This leads to the conclusion that the parallel arrangement of the tetramers is not favorable for stacking of PANI chains with singlet charge distribution.

Figure 6 presents some of the theoretically calculated electronic transitions with their wavelength and oscillator strength.

Regardless of the initial singlet charge distribution, most optimized structures produce electron spectra corresponding to higher multiplicity ground state.

In accordance with the spin-states energy splittings (Table II), the variety of allowed-spin transitions is observed first in the doubly protonated emeraldine systems. Our previous studies [31] treat some other polyaniline species, i.e., the two nonconducting forms, leucoemeraldine, neutral and monoprotonated pernigraniline, as well as the emeraldine base and the monoprotonated emeraldine salt. They all give singlet spectra in which transitions with wavelengths over 1,000 nm and oscillator strength ~0.1 typical for the triplet doubly protonated emeraldine tetramers are absent. Overall, the medium stabilizes the higher multiplicities: while the singlet transitions are abundant in the spectra in vacuum, in water they are nearly missing.

The spectra interpretation is impeded by the appearance of structures of higher multiplicity, which absorb at longer wavelengths. These types of transitions are observed first in the single singlet tetramer in vacuum but are forbidden for most of the other singlet structures in vacuum. In general, the medium effect on the spectra can be separated in two contributions. The presence of an adjacent oligomer leads to more substantial bathochromic effect of the longest wavelength transitions (LWTs) with oscillator strength of the order of 0.1 [Fig. 6(a)]. Stacking affects the singlet spectra depending on the chain alignment; i.e., stacks of greater overlap (types 1 and 3) feature transitions of longer wavelength and lower oscillator strength, whereas the displaced ones (types 2 and 4) give rise to blue-shifted more intensive lines. Hydration has adverse effect. Generally, it causes a slight hypsochromic shift of the intensive transitions, which is in line with the flattening of the structures resulting in enhanced conjugation. The most intensive lines for the hydrated species are in the range below 500 nm [Fig. 6(b)]. However, a great number of new bands of moderate and low intensity in the near and far IR region become feasible. Those located farther than 1,000 nm originate mostly from the triplet and the quintet structures.

3.2. STRUCTURES CONSTRUCTED BY TETRAMERS OF TRIPLET INITIAL CHARGE DISTRIBUTION

The molecular modeling follows the algorithm described in the previous section. The analogues of stack type 1 (frontal antiparallel), type 2 (displaced antiparallel), type 3 (frontal parallel), and type 4 (displaced parallel) are called types 5, 6, 7, and 8, respectively. The four triplet stacks are presented in Figure 7.

The chain overlap in stack type 5 is appreciable, resembling that in type 2 and unlike the one featured by the other three stacks. In terms of structural parameters, frontal and displaced antiparallel triplet configurations switch places compared with the singlet ones. Quantitative description of the geometry of these systems can be obtained from Table III.

Hydration again increases the distance between the chloride ions and the PANI skeleton; i.e., in stack types 6 and 7, they become considerable. While in the singlet stacks all $R_{H\text{—}Cl}$ are ~3 Å, in the triplet ones there are two subclasses. In stack types 5 and 8, the chloride anions are much closer. In the type 8 stack, there is marked asymmetry in the Cl^- position; i.e., two of the anions are interconnecting two tetramer chains and the others are further apart in the water ($R_{H\text{—}Cl}$ ~6 Å). This phenomenon of the chloride ions "clipping" the two

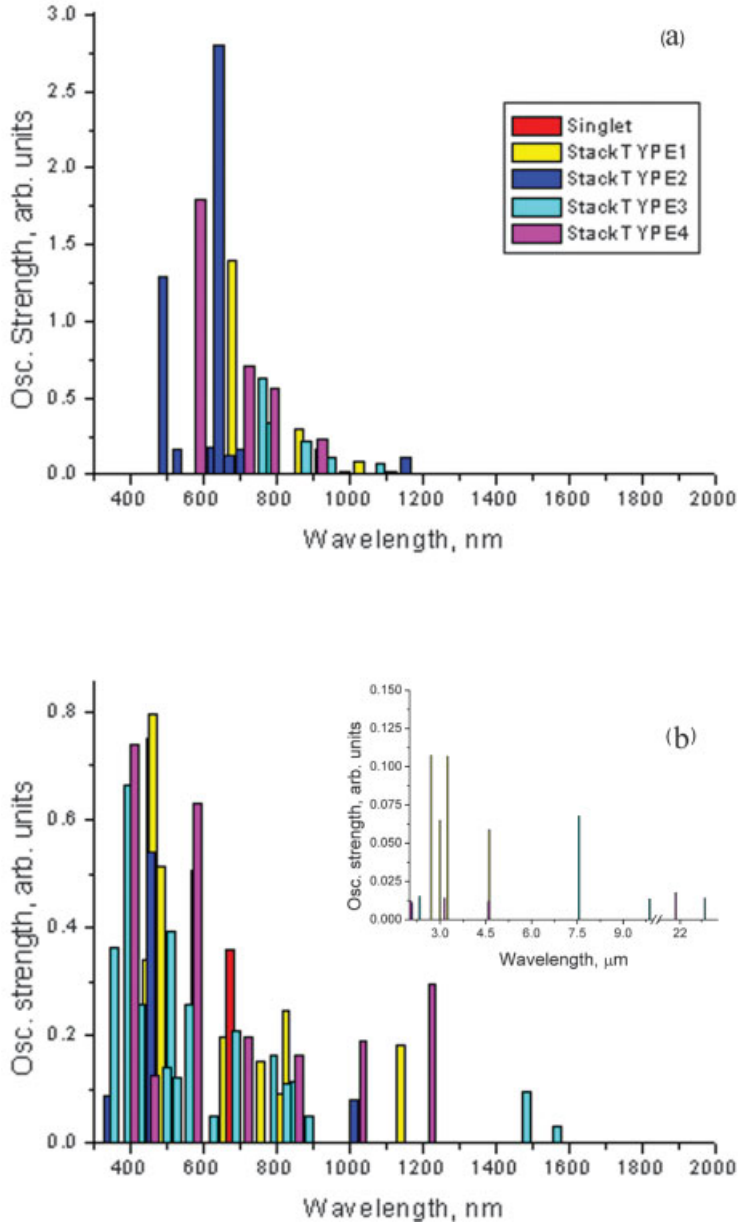

FIGURE 6. Calculated AM1/CIS UV/VIS/NIR spectra of clusters with singlet initial charge distribution: (a) in vacuum, (b) in water. Inset: transitions at >2,000 nm.

chains and holding them together is also observed in one of the mixed stacks (type 11; see the next section). In stack type 5, the proximity of the counter ions is due to the compactness of the entire structure (smallest R_{12} among the triplets). In contrast, each chloride anion in stack types 6 and 7 is interacting with a single protonated nitrogen. Generally, the water environment affects the triplet geometry less than in the singlet systems. Unlike the singlets, the presence of the second polyaniline chain increases the deformation in the parallel triplet stacks of tetramers. However, the final (averaged) values of Θ in the latter are similar to those in the singlet stacks. The intermolecular distance behavior is like that in the singlet structures; i.e., hydration draws the chains together.

The AMBER96 energy terms (Table IV) follow analogous trends as in the systems with singlet charge distribution. Once again, hydration relieves the bond tension and increases that of the torsion

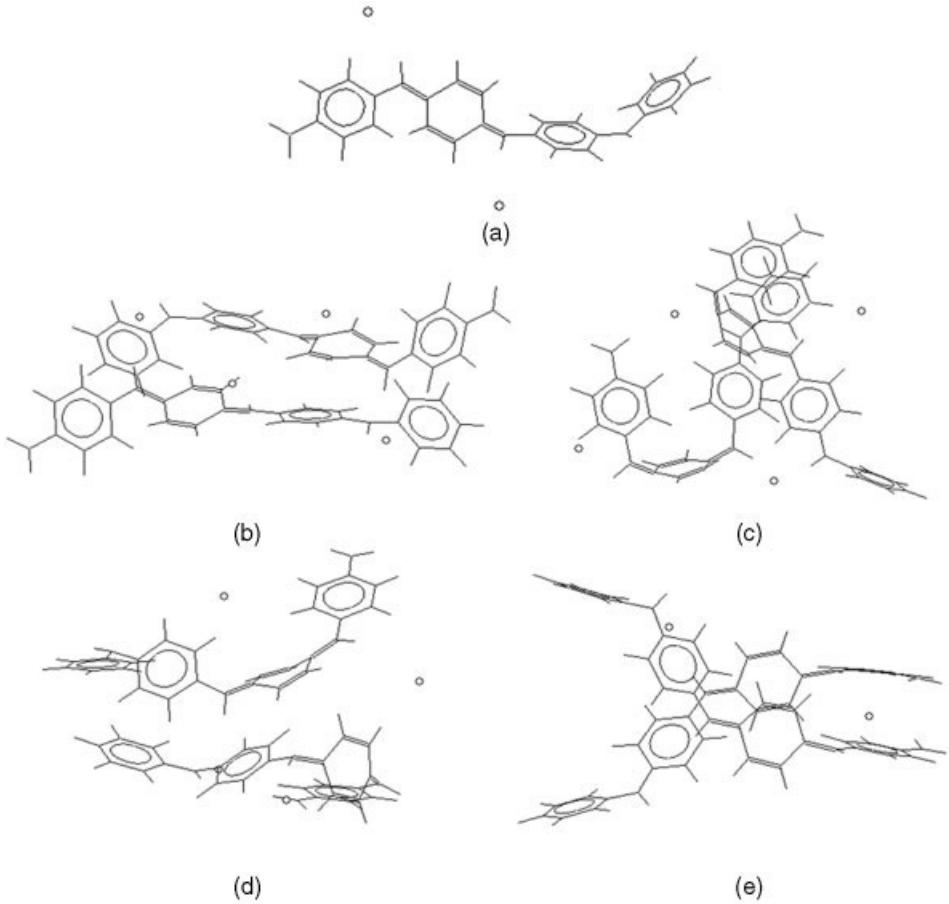

FIGURE 7. AMBER96 optimized structures of (a) a single DPE tetramer with triplet initial charge distribution and the four stacks formed by a triplet DPE tetramer pair: (b) type 5, (c) type 6, (d) type 7, and (e) type 8.

angles. The valence angles strain is also higher in aqueous environment; the van der Waals contributions are attractive on the average but less attractive than in the singlet stacks.

The values of E_{tot} prove a lower hydration effect of the triplets in comparison with their singlet analogues, and the stacks are less stable. The E_{hydr} values (Table V) correspond to much milder hydration effect; i.e., the water environment does not stabilize the triplets appreciably in general. The impact of stacking in the triplet-based systems varies from most repulsive (type 6) to most attractive (type 8) among the 12 types of stacks treated and depends strongly on the stacking pattern. Whereas the charge distribution gives preference to stacking scheme ensuring counterfacing of benzene and quinoid moieties, the optimized geometries and the values of E_{stack} reveal that for clusters containing at least one non-singlet oligomer stacking is more attractive when the quinoid fragments of the two chains are as close and as parallel as possible. Types 8 and 12 provide maximum closeness of these rings, hence, the most attractive interchain coupling.

In brief, the poorer hydration and the weaker overlap between the triplet oligomers result in lesser stabilization of the purely triplet stacks compared with those of purely singlet origin which makes them less likely. However, both are quite sensitive to chain alignment which is hardly controllable in synthetic and postsynthetic conditions/procedures.

The simulated spectra are combined in Figure 8 in the same manner as for the singlet systems in the previous section. The most intensive transition is bathochromically shifted by approximately 200 nm as compared with the singlet analogue (Fig. 6). There are no spectral lines beyond 2,000 nm, but those exceeding 1,000 nm are of much higher intensity.

Some of the tendencies observed in the previous section are preserved. The most intensive band of

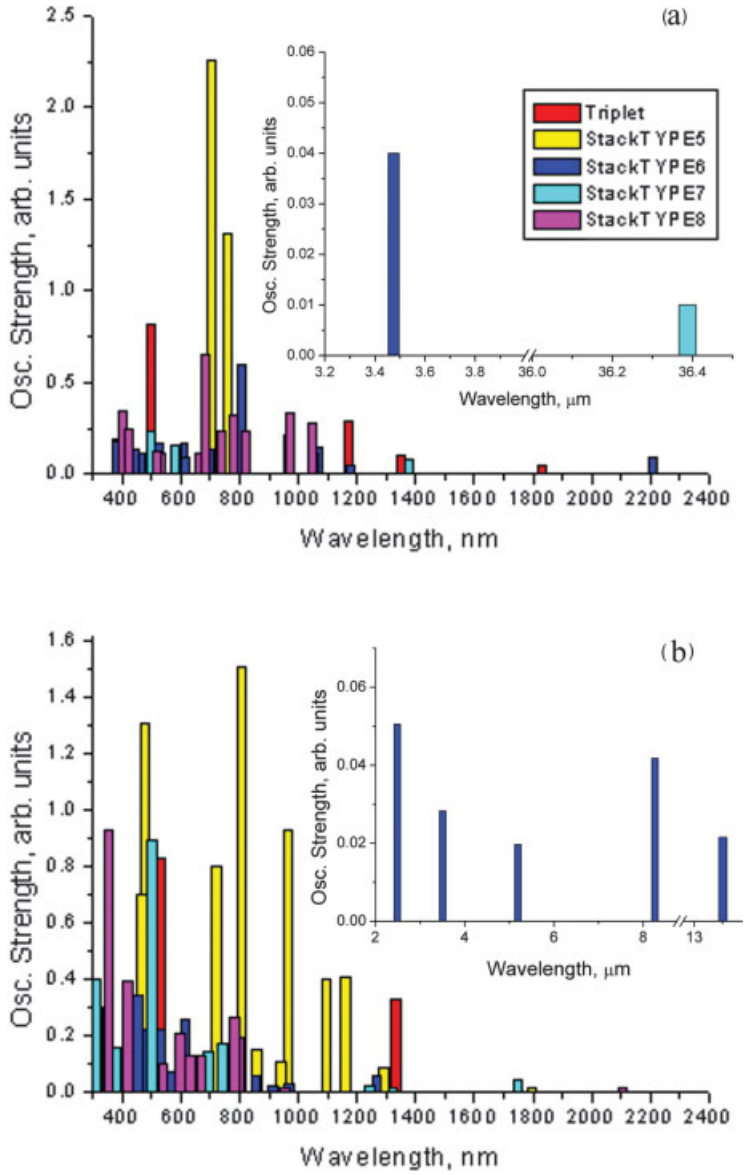

FIGURE 8. AM1/CIS calculated spectra of the structures with triplet initial charge distribution (a) in vacuum, and (b) in water.

the single triplet tetramer is at much shorter wavelength than the singlet analogue, but transitions of lower probability are found in the NIR region both in vacuum and in water. The hydration leads to slight blue shift of the longest wavelength transition of the single triplet, more pronounced for the parallel-oriented type 8. The transitions in the remaining triplet-based stacks are red-shifted especially in the antiparallel orientation. The stacking effect is ambiguous; i.e., a slight hypsochromic shift is observed in the singlet configurations of stack type 5. This effect is stronger in the last two stacks (types 7 and 8) in spite of the absent singlet structures. This is probably due to the substantial deformation of the structures, which abates conjugation in the molecules. The well-packed stack type 5 features red shift in the most intensive triplet transition accompanied by triple probability enhancement. The other triplet alignments produce bathochromically shifted lines of lower intensity. On the whole, the combined effect of stacking and hydration leads to a richer spectrum covering a broader region up to the far IR with red-shifted maxima compared with purely singlet clusters. The

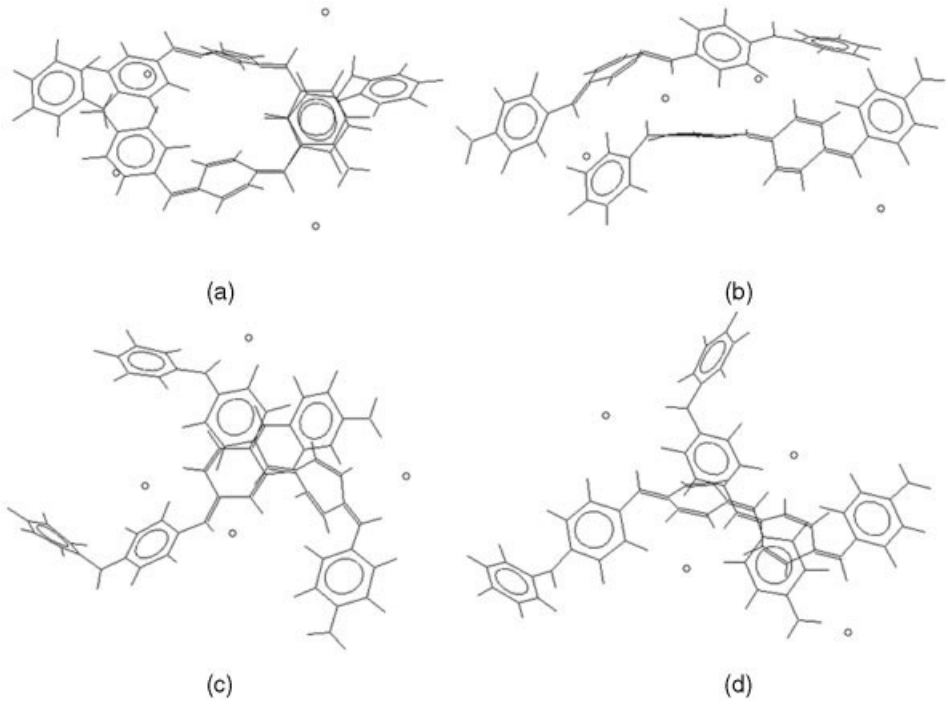

FIGURE 9. AMBER96 optimized geometries of four types of hydrated mixed stacks: (a) type 9, (b) type 10, (c) type 11, and (d) type 12.

optimized hydrated stacks 5–8 feature singlet, triplet and quintet allowed transitions with prevalence of the triplets.

3.3. MIXED STRUCTURES

In addition to the structures described in the previous sections, it is possible to create models from tetramers of different multiplicity. The mixed analogues of the already discussed stacks are called stack types 9, 10, 11, and 12, respectively (Fig. 9).

The stacks with parallel tetramer orientation are again less deformed in this series and the tetramers overlap therein is marginal. The parameter values chosen for quantitative description of the molecular geometry are presented in Table III.

Hydration leads to notable changes in the torsion angles of all structures, except the last one (type 12). Aqueous environment twists significantly stack types 9 and 10 and flattens stack type 11. As a whole, it can be seen (Fig. 9) that the mixed structures are quite deformed, stack type 11 being the only exception, and the low Θ values are a result of the compensation of opposite contributions. Two of the chloride ions in stack type 11 are shared between the protons in the neighboring chains as in stack type 7. The other counterions are pushed away between two pairs of benzene rings and invoke their divergence. Despite all these findings, as in the above-described structures, hydration draws apart the ions of contrary charge and increases the compactness of the PANI system resulting in smaller interchain distances and larger H–Cl separation.

The energy contributions are analysed based on the data in Table IV. Hydration decreases the bond strain in all stacks and increases that of the torsion and the valence angles, except in stack types 10 and 11. The substantial E_d change in stack type 12 is a proof that the aqueous environment has a very strong influence on the tetramer structure, a fact that is not well substantiated by the average Θ values. Hydration has a strong effect on the van der Waals interactions in the systems too; i.e., E_{vdw} turns negative in all cases. The stacking energy is calculated by taking into account the contributions from the tetramers of different multiplicity which build the mixed stacks. The modified relation is:

$$E_{stack} = 2 \times E_{vdw} \text{ (1 DPE in hydrated mixed stack)}$$

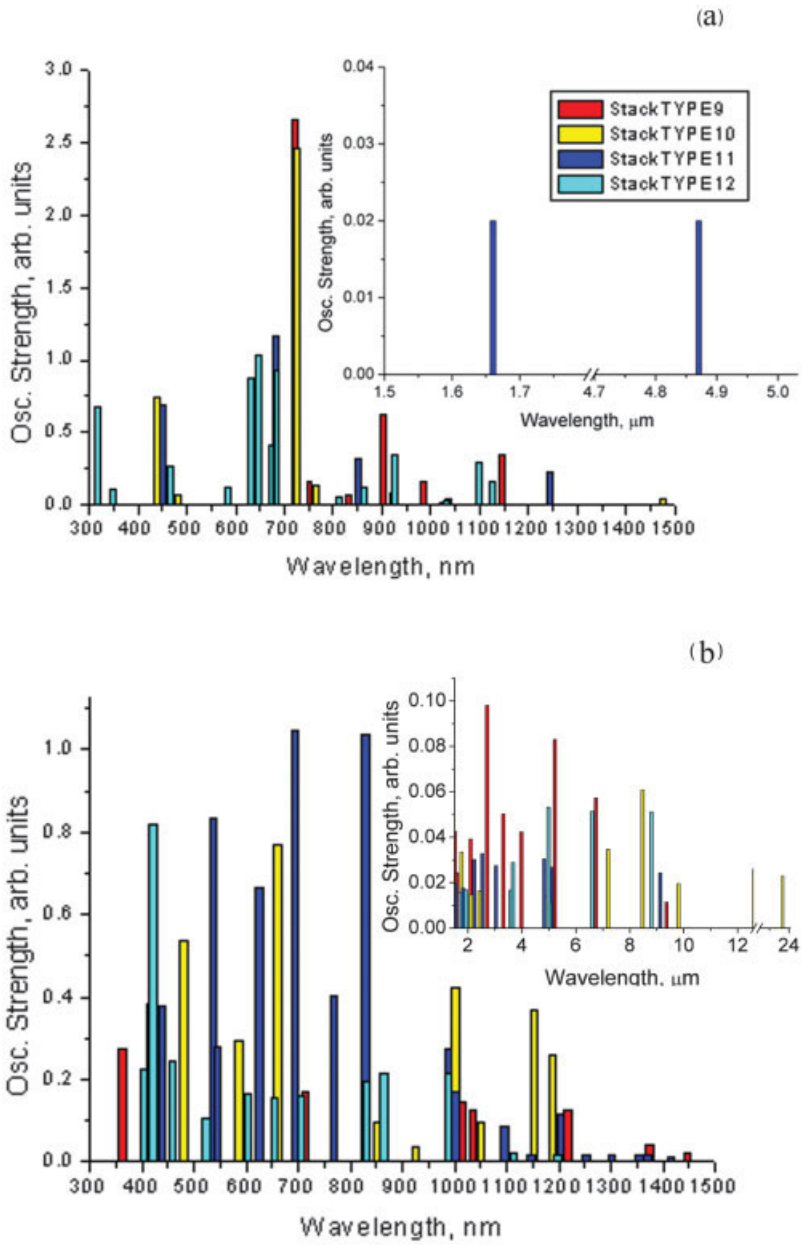

FIGURE 10. AM1/CIS calculated spectra of the structures with mixed initial charge distribution in vacuum (a) and in water (b).

$$- E_{vdw} \text{ (1 singlet hydrated DPE)}$$
$$- E_{vdw} \text{ (1 triplet hydrated DPE).} \quad (2a)$$

The calculated values for E_{stack} of stack types 9, 10, 11, and 12 (Table V) describe well the structures given in Figure 9. The tetramers overlap in stack type 11 is the worst one, hence the least attraction. The low E_{stack} of stack type 12 is probably a result of the good coincidence of the benzene and the quinoid rings in its chains and the small distance between the latter.

As expected, the total energy of the mixed systems lies between those of the singlet and the triplet stacks but the values are low enough to imply substantial share of the mixed structures in the real polymer. The hydration and stacking energies support such a prognosis (Table V). Figure 10 represents the superimposed spectra of the four mixed stacks in vacuum and in water.

Sheer stacking in vacuum leads to overall red shift, the most intensive transitions provided by the most compact stack type 10 and the longest-wavelength ones due to the loosely packed stack type 11. Hydration as usual has a slight hypsochromic effect on the most intensive peaks but gives rise to a multitude of long wavelength transitions reaching the far IR region. Actually, this spectrum is a combination of the two cases discussed previously; i.e., both the intensive transitions over 1,000 nm of the triplet systems and the "singlet" long wavelength lines of low intensity and marked strong bathochromic shift, are detected here. Interestingly, the latter are characteristic of the loosely packed stacks. A new intensive transition is noticed at 480 nm originating from the higher multiplicity structures.

The spectral characteristics of the mixed stacks show further development of the tendencies observed in the structures discussed in the first two sections. Their spectra are very rich in long wavelength lines of lower intensity. Similar transitions in the range between 1,000 and 2,000 nm are observed in almost every structure of this type including the singlet ones. Besides, many NIR and IR lines appear after spectra simulations of the mixed aggregates, which can be used in the interpretation of the conductivity in terms of existence of delocalized polarons [39]. It is worth noting that the presence of these long wavelength excitations is not an artifact of the theoretical computations; i.e., when excited states in PANI films are populated by laser irradiation, they prove to be long-lived and their emission is experimentally established with Raman-scattering of polyaniline films on mica templates [48]. Raman spectra obtained with lasers of different power and wavelength show fluorescent emission at 1,390 cm^{-1} (~7,200 nm), which is typical frequency for the delocalized polarons excitations emission in PANI, concomitant with the vibrational transition. Figure 10 shows that some of the higher multiplicity structures have transitions satisfying this condition.

3.4. FULL SPECTRUM AND MO ANALYSIS

The spectral behavior of the studied DPE clusters can be interpreted further in terms of the molecular orbital inspection.

The analysis of mixed systems energy spectra shows some resemblance to the one of the structures constructed from triplet tetramers. The highest occupied molecular orbital–lowest unoccupied molecular orbital (HOMO–LUMO) gap here is smaller, which explains the relatively prominent red-shift of the transitions. The structures that give singlet spectra absorb in the shorter wavelength range. Their LWTs are again less probable and with the participation of the chloride ions, while the most intensive ones are due to intramolecular electron transfer in the polyaniline tetramers. The higher multiplicities are characterized by more intensive long-wavelength transitions that take place between singly and doubly-occupied frontier orbitals and are intra- and intermolecular.

The main part of the highest-energy bonding orbitals of the singlet structures belongs to the chloride ions or there is a negligible contribution of polyaniline. However, in the structures of higher multiplicity a certain rearrangement can be observed; i.e., the highest bonding orbitals originate from the polyaniline chains. They are singly occupied and their number varies from two for the triplets to four for the quintets. In both cases they have very close (quasi-degenerate) energies and are localized either on the first tetramer chain or on the second one. The virtual orbitals with lowest energy are always of polyaniline nature and are located on one oligomer. Thus, the more intensive long wavelength transitions involve mainly the singly and the closest doubly occupied bonding orbitals of the triplets and the quintets. Their energy difference is smaller than the HOMO–LUMO gap and corresponds to a transition in the NIR range.

The nature of the lowest-intensity transitions obtained from triplets and quintets absorbing of $>$3,000 nm is similar for the mixed and the singlet structures LWTs in terms that chloride ions contribute significantly. The active participation of species different from the PANI chains is probably a proof that the electron density transfer between the different oligomers is accomplished with the help of low-molecular-weight mediators.

Obviously, the environment influence on the UV spectra is expressed by an assortment of different effects, including not only the PANI interactions with the water medium and the counterions, but also those with excess of monomer and other low-molecular-weight moderators, which will be the subject of another study.

The spectra shown in Figures 6, 8, and 10 are combined in Figure 11. An experimental PANI spectrum of SMNP (single-molecule nanoparticles) designed to match the theoretical models [48] is included for comparison.

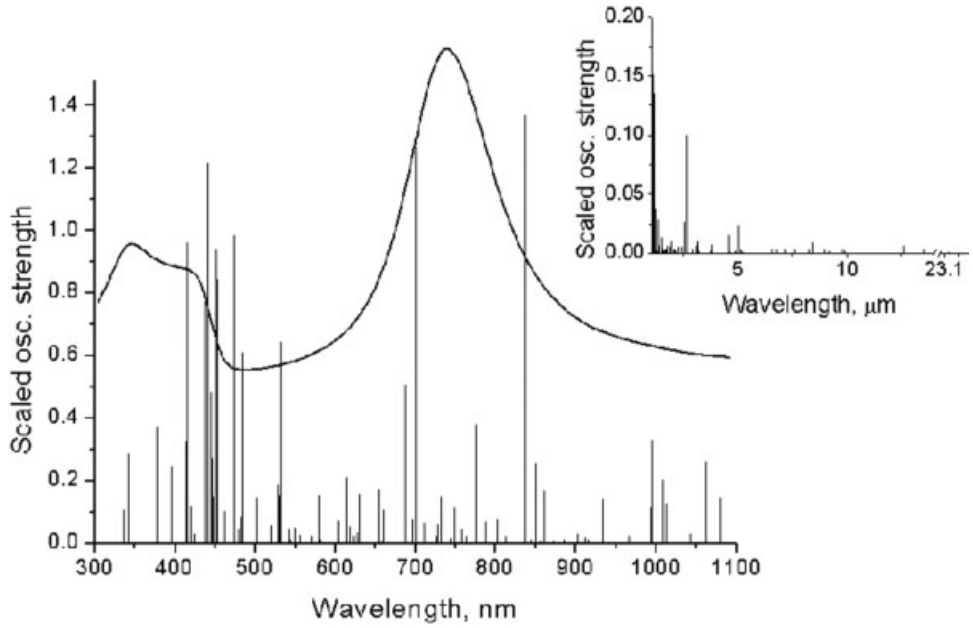

FIGURE 11. Combined spectrum of the theoretically calculated AM1/CIS transitions of all studied structures (bars) and experimental UV/VIS/NIR absorption spectrum of PANI (line) [48].

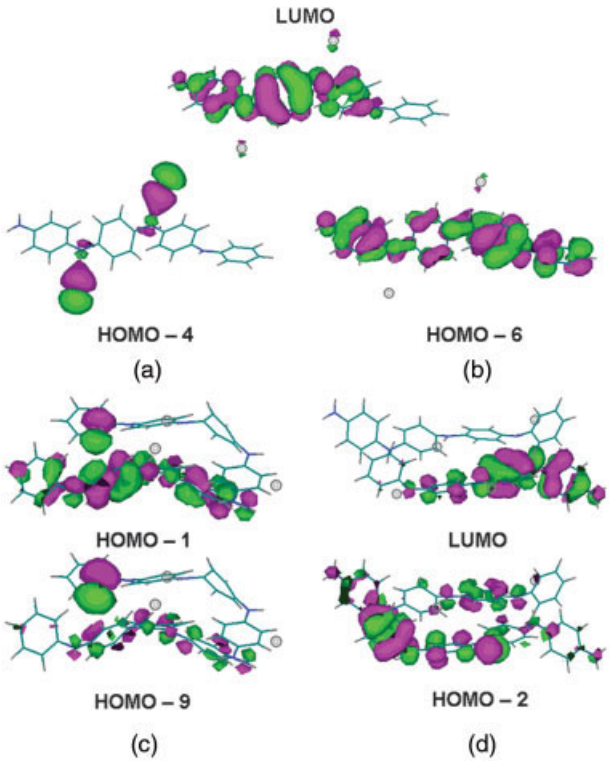

FIGURE 12. Molecular orbitals illustrating some of the possible transitions in the investigated structures: (a) $n \rightarrow \pi^*$ LWT of low intensity ($f \sim 0.01$); (b) the most intensive transition ($\pi \rightarrow \pi$); (c) intramolecular LWT ($f \geq 0.1$) between the doubly and singly occupied bonding orbitals of the high multiplicity structures; (d) intermolecular LWT ($f \geq 0.1$).

Figure 11 presents a very good agreement of theory and experiment, which can be interpreted as a proof that the chosen models are actually a close approximation to the real state of the systems. It also confirms the hypothesis for coexistence of structures with different multiplicity in the experimentally obtained emeraldine salt of PANI.

Analysis of the orbitals involved most actively in the electronic transitions shows that the studied structures feature four types of transitions (Fig. 12). The less intensive spectral lines ($f \sim 0.01$) originate from electron transfer between the chloride anions and the polyaniline part of the system [Fig. 12(a)], i.e., to a $n \rightarrow \pi^*$ transition. The most intensive transitions ($f \sim 1.0$) in the UV/VIS/NIR range take place between molecular orbitals with predominant PANI share ($\pi \rightarrow \pi^*$ transition). The electron density in these cases is shifted from the benzene rings to the quinoid one [Fig. 12(b)].

The presence of two polyaniline chains in the stacks raises the question whether the electronic transition is intra- or intermolecular. The most intensive LWTs ($f \geq 0.1$) for the major part of the stacks are due to a mixed $n \rightarrow \pi^*$ and intramolecular $\pi \rightarrow \pi^*$ electron transfer [Fig. 12(c)]. In some of the structures, intermolecular $\pi \rightarrow \pi^*$ transitions are observed [Fig. 12(d)].

TABLE VI
Statistical distribution of the studied structures according to their AM1/CIS multiplicity.

Type	Multiplets			
	Total	Singlets	Triplets	Quintets
Singlet vacuum	1	1	—	—
Triplet vacuum	1	—	1	—
Stack type 1 vacuum	2	1	1	—
Stack type 2 vacuum	2	1	1	—
Stack type 3 vacuum	2	1	1	—
Stack type 4 vacuum	2	1	1	—
Stack type 5 vacuum	1	1	—	—
Stack type 6 vacuum	3	—	2	1
Stack type 7 vacuum	1	1	—	—
Stack type 8 vacuum	3	1	1	1
Stack type 9 vacuum	2	1	—	1
Stack type 10 vacuum	2	1	1	—
Stack type 11 vacuum	2	—	1	1
Stack type 12 vacuum	3	1	1	1
Singlet water	12	—	12	—
Triplet water	16	—	16	—
Stack type 1 water	39	1	32	6
Stack type 2 water	23	2	19	2
Stack type 3 water	22	—	20	2
Stack type 4 water	16	1	16	—
Stack type 5 water	33	3	18	12
Stack type 6 water	37	—	22	15
Stack type 7 water	16	—	16	—
Stack type 8 water	30	—	16	14
Stack type 9 water	34	—	23	11
Stack type 10 water	17	1	15	1
Stack type 11 water	36	16	12	8
Stack type 12 water	26	—	24	2
Sum total:	384	35	271	78

The longest wavelength absorption of the systems is a subject of practical interest. Possibly, it is responsible for the protonated emeraldine systems conductivity, while their green color is due to the highest intensity spectral lines of shorter wavelength (~800 nm). The analysis of the higher intensity long wavelength transitions ($\lambda \geq 1{,}000$ nm, oscillator strength 0.1) and the molecular orbitals involved in these show that they result from the higher multiplicity structures. Therefore, the latter are very important, as they would be responsible for the conducting properties of polyaniline. Their share in the studied systems is substantial as evidenced by the data in Table VI.

384 theoretically simulated UV spectra were used in this study. The averaging is performed over 1301 spectral lines.

4. Summary

Comparative analysis of the obtained results shows that:

1. Definite multiplicity cannot be specified for the ground state of the emeraldine salt. Low- and high-spin electron configurations of almost equal probability are feasible both in vacuum and in aqueous medium. The latter certainly stabilizes the high-spin states, whereas the aggregation favors intermediate multiplicity values. Pronounced stability is typical for magnetically inactive and mixed clusters while stacks of purely high-spin chains are less realistic.
2. The most sensitive structural parameter, the average dihedral angle, Θ, depends on the spin-states of the components in the cluster and on the presence of solvent. Compared with its value for single chains, Θ decreases in singlet aggregates, increases in high-spin ones and rests unchanged in the mixed stacks. Hydration flattens the singlets, mildly deforms the triplets and substantially twists the mixed structures.
3. In all cases, hydration enhances the interchain van der Waals interaction and the counterions separation. Displaced singlets feature best hydration, whereas displaced mixed stacks have the tightest packing. Proximity of quinoid parallel rings is usually related to good overlap of a chain portion and quite poor in the adjacent chain sectors. The stacks with most attractive van der Waals interaction are an appropriate illustration but they give rise to short-wavelength transitions in the electronic spectra. In contrast, the systems with second-to-best E_{vdw} produce quite long-wavelength lines. In an attempt to generalize to real polymer chains, this would imply that tightly packed sections will be surrounded by disordered chain segments, the moderate van der Waals attraction providing better crystallinity. The presence of water in PANI assemblies would also facilitate ordering.
4. Electronic transitions are intramolecular in low-spin clusters; both intra- and intermolecular transitions are possible in high-spin stacks. Counterions play key role in spectral behaviour. The simulated electronic spectra

cover a broad range from UV to NIR and IR regions. Low-spin clusters absorb at about 800 nm whereas medium and high-spin aggregates have maxima at shorter wavelengths but give rise to a large number of comparatively intensive long-wavelength transitions.

In conclusion, the proposed theoretical models allow a number of qualitative and semi-quantitative estimates on energetic and optical characteristics of emeraldine salt in vacuum and in aqueous solution, which can provide an explanation of hydration and stacking effects in PANI.

ACKNOWLEDGMENTS

The authors acknowledge the grants of the Organizing Committee for participation in the Third Humboldt Conference on Computational Chemistry. Thanks are due to Ph. Shushkov and R. Tadjer for technical help.

References

1. Annis, B. K.; Specht, E. D.; Theophilou, N.; MacDiarmid, A. G. Polymer 1991, 32, 1160.
2. Monkman, A. P.; Adams, P. Solid State Commun 1991, 78, 1.
3. Sariciftci, N. S.; Heeger, A. J.; Cao, Y. Phys Rev B 1994, 49, 5988.
4. Pron, A.; Rannou, P. Prog Polym Sci 2002, 27, 135.
5. Masters, J. G.; Ginder, J. M.; MacDiarmid, A. G.; Epstein, A. J. J Chem Phys 1992, 96, 4768.
6. Ghosh, S. Chem Phys Lett 1994, 226, 344.
7. Oka, O.; Kiyohara, O.; Yoshino, K. Jpn J Appl Phys 1991, 30, L653.
8. http://www.cea.fr/fr/Publications/clefs44/fr-clefs44/clefs4489.htm.
9. Aldissi M., Ed. Intrinsically Conducting Polymers: An Emerging Technology; NATO-ASI Series; Vol. E246; Kluwer: Dordrecht, the Netherlands, 1992.
10. Miller, J Adv Mater 1993, 5, 671.
11. Kulkarni, V. G.; Mathew, R.; Campbell, J. C. Synth Met 1993, 55–57, 3780.
12. Ginder, J. M.; Epstein, A. J. Phys Rev B 1990, 41, 10674.
13. Ginder, J. M.; Epstein, A. J.; MacDiarmid, A. G. Solid State Commun 1989, 72, 987.
14. Brédas, J. L.; Quattrocchi, C.; Libert, J.; MacDiarmid, A. G.; Ginder, J. M.; Epstein, A. J. Phys Rev B 1991, 44, 6002.
15. Brédas, J. L. Proceedings of the Nobel Symposium on Conjugated Polymers and Related Materials: The Interconnection of Chemical and Electronic Structure; Oxford University Press: Oxford, 1992, p 187.
16. McCall, R. P.; Ginder, J. M.; Leng, J. M.; Coplin, K. A.; Ye, H. J.; Epstein, A. J.; Asturias, G. E.; Manohar, S. K.; Masters, J. G.; Scheer, E. M.; Sun, Y.; MacDiarmid, A. G. Synth Met 1991, 41/43, 1329.
17. Djurado, D.; Bee, M.; Gonzalez, M.; Mondelli, C.; Dufour, B.; Rannou, P.; Pron, A.; Travers, J. P. Chem Phys 2003, 292, 355.
18. Schreiber, M.; Tenelsenb, K.; Vojta, T. J. Luminescence 1996, 66/67, 521.
19. Aoki, K.; Teragishi, Y. J. Electroanal Chem 1998, 441, 25.
20. Wennerstrom, O. Macromolecules 1985, 18, 1977.
21. Libert, J.; Cornil, J.; dos Santos, D. A.; Bredas, J. L. Phys Rev B 1997, 56, 8638.
22. Barta, P.; Kugler, Th.; Salaneck, W. R.; Monkman, A. P.; Libert, J.; Lazzaroni, R.; Bredas, J. L. Synth Met 1998, 93, 83.
23. Grossmann, B.; Heinze, J.; Moll, T.; Palivan, C.; Ivan, C.; Gescheidt, G. J Phys Chem B 2004, 108, 4669.
24. Foreman, J. P.; Monkman, A. P. J. Phys Chem A 2003, 107, 7604.
25. Jansen, S. A.; Duong, T.; Major, A.; Wei, Y.; Sein, L. T. Synth Met 1999, 105, 107.
26. Vaschetto, M. E.; Retamal, B. A. J Phys Chem A 1997, 101, 6945.
27. Choi, C. H.; Kertesz, M. Macromolecules 1997, 30, 620.
28. Boyer, M. I.; Quillard, S.; Louarn, G.; Lefrant, S. Synth Met 1999, 101, 782.
29. Oliveira Z.; dos Santos, M. C. Chem Phys 2000, 260, 95.
30. Ikkala, O. T.; Pietilä, L.-O.; Ahjopalo, L.; Österholm, H.; Passiniemi, P. J. J Chem Phys 1995, 103, 9855.
31. Ivanova, A.; Madjarova, G.; Tadjer, A.; Gospodinova, N. Int J Quantum Chem 2006, 106, 1383.
32. Krinichnyi, V. I.; Chemerisov, S. D.; Lebedev, Ya. S. Phys Rev B 1997, 55, 16233.
33. Krinichnyi, V. I.; Roth, H.-K.; Hinrichsen, G.; Lux, F.; Lueders, K. Phys Rev B 2002, 65, 1552051.
34. Hopkins, A. R.; Rasmussen, P. G.; Basheer, R. A. Macromolecules 1996, 29, 7838.
35. Langer, J. J.; Krzyminiewski, R.; Kruczynski, Z.; Gibinski, T.; Czajkowski, I.; Framski, G. Synth Met 2001, 122, 359.
36. Male, R.; Allendoerfer, R. D. J Phys Chem 1988, 92, 6237.
37. Tang, J.; Allendoerfer, R. D.; Osteryoung, R. A. J Phys Chem 1992, 96, 3531.
38. Heuvelen, A. V.; Goldstein, L. J Phys Chem 1968, 72, 481.
39. MacDiarmid, A. G.; Epstein, A. J. Synth Met 1995, 69, 85.
40. Coplin, K. A.; Jasty, S.; Long, S. M.; Manohar, S. K.; Sun, Y.; MacDiarmid, A. G.; Epstein, A. J. Phys Rev Lett 1994, 72, 3206.
41. Joo, J.; Long, S. M.; Pouget, J. P.; Oh, E. J.; Macdiarmid, A. G.; Epstein, A. J. Phys Rev B 1998, 57, 9567.
42. Karabunarliev, S.; Baumgarten, M.; Mullen, K. J Phys Chem A 1998, 102, 7029.
43. (a) Weiner, S. J.; Kollman, P. A.; Case, D. A.; Singh, U. C.; Ghio, C.; Alagona, G.; Profeta, S., Jr.; Weiner, P. J Am Chem Soc 1984, 106, 765; (b) Weiner, S. J.; Kollman, P. A.;

Nguyen, D. T.; Case, D. A. J Comput Chem 1986, 7, 230; (c) Cornell, W. D.; Cieplak, P.; Bayly, C. I.; Gould, I. R.; Merz, K. M.; Jr.; Ferguson, D. M.; Spellmeyer, D. C.; Fox, T.; Caldwell, J. W.; Kollman, P. A. J Am Chem Soc 1995, 117, 5179.

44. Petrov, G. Organic Chemistry; Sofia University Press/St. Kl. Ohridski: Sofia, 1996.
45. Zoppellaro, G.; Ivanova, A.; Enkelmannn, V.; Geies, A.; Baumgarten, M. Polyhedron 2003, 22, 2099.
46. HyperChem 7.0; Hypercube: Gainesville, FL, 2002.
47. Stewart, J. J. P. MOPAC: A General Molecular Orbital Package; Version 7.2; QCPE: Bloomington, IN, 1995.
48. Gospodinova, N.; Dorey, S.; Zhekova, H.; Ivanova, A.; Tadjer, A. J Mat Chem (submitted).